Research Article Vol. 57, No. 10 / 1 April 2018 / Applied Optics C83

applied optics

Acousto-optic filters based on the superposition of diffraction fields [Invited]

V. M. Kotov,* S. V. Averin, E. V. Kotov, and G. N. Shkerdin

Kotel'nikov Institute of Radio Engineering and Electronics (Fryazino Branch), Russian Academy of Sciences, Fryazino, Moscow Region 141190, Russia
**Corresponding author: vmk6054@mail.ru*

Received 26 October 2017; revised 29 January 2018; accepted 29 January 2018; posted 30 January 2018 (Doc. ID 310116); published 23 February 2018

Methods for the calculation of the acousto-optic (AO) transfer functions forming as a result of superposition of two AO fields with similar and orthogonal light polarizations are proposed. Specific calculations are made on the basis of the parameters widely used in practice with uni-axial gyrotropic crystal paratellurite. It is revealed that the resulting field is generally very inhomogeneous but contains domains with two-dimensional behavior properties. These domains can be used for two-dimensional image edge enhancement based on Fourier processing. Theoretical conclusions are verified by means of the optical image Fourier processing with the spatial frequency AO paratellurite filters. © 2018 Optical Society of America

OCIS codes: (070.2615) Frequency filtering; (070.1060) Acousto-optical signal processing; (070.6110) Spatial filtering.

https://doi.org/10.1364/AO.57.000C83

1. INTRODUCTION

Acousto-optic (AO) is one of the effective methods for controlling of optical radiation parameters such as amplitude, phase, frequency, direction of the light propagation, etc. [1–4]. It was found that angular spectrum of the diffracted light is determined by the divergences of the light and sound and sound power [5,6]. It was also found that AO can successfully process the optical images [7,8]. One of the promising applications of the AO cells is their use in the optical Fourier processing systems. For the first time AO elements were considered as the spatial frequency filters in [9]. The conditions were revealed in which the AO elements can operate as the linear spatial filters. After that, several publications were devoted to the investigation of the transfer functions properties (see, for example, [10,11]). Bragg diffraction image edge enhancement was demonstrated for the first time theoretically and experimentally in [12]. The edge enhancement is one of the basic operations of the optical image processing because it sufficiently decreases the processing information but at the same time keeps very important object characteristics such as form and dimensions [13,14]. These characteristics help to make the identification of the object and observe its movement, rotation, etc.

Traditionally, AO interaction is one-dimensional (1D), therefore it allows performing only 1D image processing. The 1D processing on the basis of a single AO element and two-dimensional (2D) processing with two orthogonally oriented AO cells is demonstrated in [15]. For essential improving of the 1D image contour, it is suggested the use of two cascaded acousto-optic cells with contra-propagating sound [16]. Notch spatial filtering with an acousto-optic modulator was also proposed in [17]. Extensive investigation of all possible options of AO diffraction for the image edge enhancement was implemented in [18–23]. Among all versions, two cases were extracted that allow processing of 2D images: collinear diffraction [18,20,21,23] and tangent geometry of diffraction [20–22] when the tangential planes drown to the wave vector surfaces in the crossing points of the wave vectors of incident and diffracted beams are parallel each other [24].

In all cases mentioned above, it is assumed that only one beam keeping the information is involved into diffraction process. This beam diffracts into the first diffraction order.

In our paper, we are considering more complicated cases when the transfer functions form as a superposition of two AO fields. It occurs, for example, during multi-phonon Bragg diffraction, or in the case when two eigenmodes of crystal take part in the diffraction process.

It will be shown that the proposed versions are suitable for 2D image edge enhancement. The theoretical considerations of these options appear more complicated in comparison with the "common" Bragg diffraction into one order, but for all that, the experimental realization of new cases is no more intricate at all. The proposed options significantly extend the opportunities of the AO interaction for image processing.

2. TRANSFER FUNCTION AS A SUPERPOSITION OF TWO FIELDS WITH SIMILAR POLARIZATIONS

Several models of AO diffraction considering the ellipticity of eigenwaves propagating in a TeO_2 crystal have been developed (see, for example, [3,25–27]). However, the equations in these papers did not take into account the gyrotropy of the AO crystal.

In our approach, we consider AO diffraction taking into account both ellipticity of eigenmodes and the spatial curvature of a wave vector surfaces of the gyro tropic crystal.

We start with wave equation for a dielectric crystal,

$$\mathrm{rot}[\mathrm{rot}\,\mathbf{E}] + 1/c^2 \frac{\partial^2 \mathbf{D}}{\partial t^2} = 0, \tag{1}$$

where $\mathbf{E}$ and $\mathbf{D}$ are vectors of electric field and induction in the crystal; c is speed of light in vacuum. The expression for a component of dielectric tensor ε_{ik} in the material equation $D_i = \varepsilon_{ik}E_k$, where D_i and E_k are the components of vectors $\mathbf{D}$ and $\mathbf{E}$, respectively, is written in the form (see, for example, [27])

$$\varepsilon_{ik} = \varepsilon^0_{ik} + ie_{ikl}G_l - \varepsilon^0_{il}\varepsilon^0_{km}p_{\mathrm{lm}nj}u_{nj}. \tag{2}$$

Here, ε^0_{ik} are the components of unperturbed dielectric permittivity, G_l are the components of an axial gyration vector, e_{ikl} is the Levi–Civita symbol, p_{lmnj} are the components of the tensor of photo elasticity, u_{nj} are the components of a crystal strain tensor related to the ultrasonic wave (the additives to the dielectric function due to gyrotropy and photo elasticity are assumed small). The components of the gyration vector may be expressed in terms of components of gyration pseudo-tensor G_{ij}:$G_i = G_{ij}s_j$, where s_j are the components of a unit vector $\mathbf{s}$ of a plane wave propagating parallel to the wave vector $\mathbf{k}(\mathbf{k} = k\mathbf{s})$. Further calculations will refer to the uniaxial crystal of tellurium dioxide (TeO_2), which has a point symmetry group 422. In the basic system of coordinates of paratellurite, we have $\varepsilon^0_{xx} = \varepsilon^0_{yy} = \varepsilon_1$, $\varepsilon^0_{zz} = \varepsilon_3$, $G_{xx} = G_{yy} = G_{11}$, and $G_{zz} = G_{33}$. We assume also that an electromagnetic wave propagates across the crystal at sufficiently small angles with respect to the optical axes; in this case the effect of gyrotropy is important.

Calculation of AO interaction by solving wave Eq. (1) is simpler if one uses the coupled-mode approach with slowly varying wave amplitudes. Without an ultrasonic wave, a solution for the electric induction vector $\mathbf{D}(\mathbf{r})$ for every propagation direction $\mathbf{s}$ is given by a linear combination of two orthogonal elliptically polarized Eigen modes:

$$\mathbf{D}(\mathbf{r}) = B_1\mathbf{b_1}e^{ik_1\mathbf{sr}} + B_2\mathbf{b_2}e^{ik_2\mathbf{sr}}, \tag{3}$$

where B_1, B_2 are the constants responsible for the contributions of each mode into the induction, and

$$\mathbf{b}_1 = \frac{\mathbf{e}_1 + i\rho\mathbf{e}_2}{\sqrt{1+\rho^2}}, \qquad \mathbf{b}_2 = \frac{\mathbf{e}_2 + i\rho\mathbf{e}_1}{\sqrt{1+\rho^2}}, \tag{4}$$

where $\mathbf{e}_1$ and $\mathbf{e}_1$ are the unit vectors directed along main axes of a central cross section of the crystal indicatrix by a wave-front plane, which is determined by vector $\mathbf{s}$ (vector $\mathbf{e}_1$ is directed along the short axis of the ellipse and $\mathbf{e}_1$-along the long axis); ρ is the ellipticity of eigenmode polarization, i.e., the ratio of short to long axis lengths of the polarization ellipse; and k_1 and k_2 are the absolute values of the wave vectors of eigenmodes. Ellipticity ρ and the absolute values k_1 and k_2 of the wave vectors are given by known relations [27–29].

Expression similar to Eq. (3) can also be written for the electric field vector $\mathbf{E}(\mathbf{r})$ where the ellipticity of eigenmodes in the plane of the wave front coincides with ellipticity ρ in Eq. (3), however, there is a small longitudinal field component in this equation [28].

Let us assume that the slow shear acoustic wave propagates in the [110] direction and causes mechanical deformation perpendicular both to the crystal optical axis and to direction of wave propagation. We may transfer from the basic system of coordinates [100], [010], [001] to the system of coordinates xyz where the axis x is parallel to $[1\bar{1}0]$, y is parallel to [110], and z is parallel to [001]. In this case AO interaction is described by a single photo elastic constant $\tilde{p}_{66} = (p_{11} - p_{22})/2$, where p_{11}, p_{22} are the components of photoelastic tensor in double-index notation.

We will consider now double AO interaction describing the zeroth and second diffraction orders by the solution branches with the greater refraction index. Then, with neglected gyrotropy, the optical radiation will be represented by the extraordinary beams. We will describe the first diffraction order by the solution branch with the smaller refraction index, in this case radiation may be presented by ordinary beam. The expressions for the electric fields in the diffraction orders $\mathbf{E}_m(\mathbf{r})$ are written in the form of

$$\mathbf{E}_m(\mathbf{r}) = V_m(z)\mathbf{b}_m e^{ik_{mz}z + ik_{0x}x + i(k_{0y}+mq)y - i\omega_m t}, \tag{5}$$

where $m = 0, 1, 2$ is the diffraction order number; i is the mode number ($i = 1$ corresponds to the slower mode, $i = 2$ corresponds to the faster mode); k_{0x} and k_{0y} are the wave vector projections of the incident electromagnetic wave onto the axis x and y; k_{mz} is the z component of the wave vector for the corresponding eigenmode described by the vector $\mathbf{b}_m$; $\omega_m = \omega + m\Omega$, where ω and Ω are the angular frequencies of electromagnetic and ultrasonic waves, respectively.

At the presence of ultrasonic waves, the amplitudes of eigenmodes satisfying Bragg synchronism conditions are slow functions of coordinates. By neglecting the longitudinal components of the electric field, we may derive a system of truncated equations for the amplitudes obtained from the orthogonality of eigenmodes in the wave-front plane (see, for example, [28]).

The resulting system of equations for diffraction orders $V_m(z)$ is

$$\begin{aligned}
\frac{dV_0}{dz} &= i\gamma_1^* e^{i\Delta k_1 z}V_1,\\
\frac{dV_1}{dz} &= i\gamma_1 e^{-i\Delta k_1 z}V_0 + i\gamma_2 e^{i\Delta k_2 z}V_2,\\
\frac{dV_2}{dz} &= i\gamma_2^* e^{-i\Delta k_2 z}V_1,
\end{aligned} \tag{6}$$

where the asterisk means the complex conjugation; $\gamma_{1,2} = \frac{k^2\Delta\varepsilon_{1,2}f_{10,21}}{2k_{0z}}$ are the coupling constants with $\Delta\varepsilon_1 = -1/2q\varepsilon_1^2\tilde{p}_{66}Ae^{-i\varphi}$ and $\Delta\varepsilon_2 = \Delta\varepsilon_1^*$, where A and q are the amplitude and absolute value of the ultrasound wave vector; φ is

the phase of the ultrasound wave; f_{10} and f_{21} are the coefficients describing influence of eigenwave ellipticity on the diffraction process; and Δk_1 and Δk_2 are vectors of Bragg synchronism mismatch. Expressions for f_{10} and f_{21} are rather cumbersome even at small angles between the radiation propagation direction and crystal optical axes [30].

In the case where the polarization of eigenmodes is almost circular, we have [30]

$$|f_{10}| \approx \frac{1+\rho_0\rho_1}{\sqrt{(1+\rho_0^2)(1+\rho_1^2)}},$$
$$|f_{21}| \approx \frac{1+\rho_2\rho_1}{\sqrt{(1+\rho_2^2)(1+\rho_1^2)}}. \quad (7)$$

Here ρ_0, ρ_1, ρ_2 are the ellipticities of eigenmodes for zeroth, first, and second orders, respectively. Expressions for the coupling constants $\gamma_{1,2}$ may be written in the form of $\gamma_{1,2} = (\nu/2L) f_{10,21}$, where ν is the Raman–Nath parameter [3], $\nu = \frac{2\pi}{\lambda}\sqrt{\frac{M_2 L}{2H} P_{ac}}$, where λ is the light wavelength; L and H are the length and height of the acoustic column; M_2 is AO figure of merit, $M_2 \approx \frac{n_0^6 P_{ef}^2}{dV^3}$, where n_0 is refractive index and d and V are the density of the material and acoustic velocity and P_{ef} is effective elasto-optic constant. In our case, $P_{ef} = 0.5(p_{11} - p_{12})$. For linear ($\rho_{0,1,2} = 0$) and circular ($\rho_{0,1,2} = 1$) polarizations we obtain $f_{10,21} = 1$, and Eqs. (5)–(7) transfer to well-known expressions (see, for example, [1–3]). Note that system of Eqs. (5)–(7) describes an experimental situation where the intensities of the radiation diffracted into different orders determined by the functions $|V_m(z)|^2$, which are experimentally measured.

For the processing of 2D images we considered a three-dimensional model of the wave vector surfaces taking into account the angular mismatch of Bragg scattering both in the diffraction plane and in the orthogonal plane. Figure 1 shows three-dimensional vector diagram of two-phonon Bragg diffraction in a uni-axial positive gyrotropic crystal TeO_2.

Here, S_1 and S_2 are the wave-vector surfaces of ordinary and extraordinary beams, respectively. The Z axis coincides with the optical axis of the crystal; the acoustic wave with the wave vector $\mathbf{q}$ is directed along the X axis. Let us assume that incident beam with the wave vector $\mathbf{k}_0$ is directed to the point A_0 lying at the intersection of the plane XZ and the surface S_2. As a result of the AO interaction with the acoustic wave $\mathbf{q}$, the beam $\mathbf{k}_0$ successively diffracts in the direction of the beams whose wave vectors are directed to points A_1 and A_2. Point A_1 lies on the surface S_1, while point A_2 lies on the surface S_2. The case of anisotropic diffraction has occurred. Both acts of diffraction take place in the regime of strong Bragg synchronism. If now the beam $\mathbf{k}_0$ is inclined at an angle α to the plane XZ, i.e., propagates in the direction of the beam $\mathbf{k}_0^1$ directed to the point A_0, it successively diffracts during the interaction with the same acoustic wave in the direction of the beams whose wave vectors are directed to points B_1 and B_2. However, diffraction acts are accompanied by Bragg synchronism mismatch. The mismatch vectors are denoted in Fig. 1 as $\Delta\mathbf{k}_1$ and $\Delta\mathbf{k}_2$.

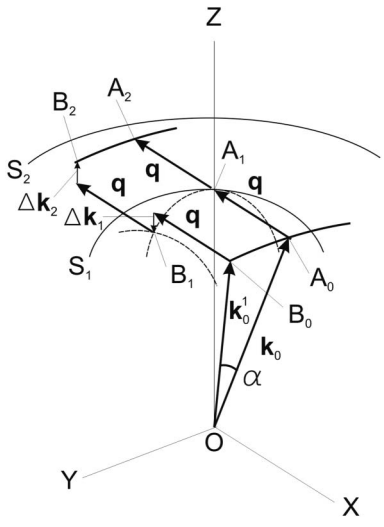

Fig. 1. Three-dimensional diagram of two-phonon Bragg diffraction in uni-axial positive gyrotropic crystal TeO_2.

For the calculations in the case of TeO_2 crystal, we used a model where refractive indices were equal to [31,32]

$$n_{1,2}^2 = \frac{1+tg^2\varphi}{\frac{1}{n_0^2} + \frac{tg^2\varphi}{2}\left(\frac{1}{n_0^2}+\frac{1}{n_e^2}\right) \pm \frac{1}{2}\sqrt{tg^4\varphi\left(\frac{1}{n_0^2}-\frac{1}{n_e^2}\right)+4G_{33}^2}} \quad (8)$$

and ellipticity of the optical beam is

$$\rho = \frac{1}{2G_{33}}\left[\sqrt{tg^4\varphi\left(\frac{1}{n_0^2}-\frac{1}{n_e^2}\right)^2 + 4G_{33}^2} - tg^2\varphi\left(\frac{1}{n_0^2}-\frac{1}{n_e^2}\right)\right], \quad (9)$$

where n_0 and n_e are the principal refractive indices of the crystal; φ is the angle between the optical axis of the crystal and the wave vector of the light wave; and G_{33} is the component of the gyration pseudo-tensor. The parameters that were used for calculations corresponded to the wavelength $\lambda = 0.63$ μm, $n_0 = 2.26$, $n_e = 2.41$, $G_{33} = 2.62 \times 10^{-5}$.

Equation (8) allows one to determine the surfaces of the light wave vectors in Cartesian coordinates [32],

$$k_z^4\left(\frac{1}{k_0^4} - \left(\frac{\lambda}{2\pi}\right)^4 G_{33}^2\right) + (k_x^2+k_y^2)\left(\frac{1}{k_0^2}+\frac{1}{k_e^2}\right)\left(\frac{k_z^2}{k_0^2}-1\right) + \frac{(k_x^2+k_y^2)^2}{k_0^2 k_e^2} - \frac{2k_z^2}{k_0^2} + 1 = 0, \quad (10)$$

where $k_0 = 2\pi n_0 \lambda^{-1}$; $k_e = 2\pi n_e \lambda^{-1}$; λ is wavelength; and k_x, k_y, and k_z are the projections of optical wave vector $\mathbf{k}$ onto axes X, Y, and Z, respectively. Note that Eq. (10) is a fourth-order equation. If gyrotropy is absent, this expression is reduced to two second-order equations. Indeed, at $G_{33} = 0$ it transforms into

$$\left(\frac{k_z^2}{k_0^2}-1\right)^2 + (k_x^2+k_y^2)\left(\frac{1}{k_0^2}+\frac{1}{k_e^2}\right)\left(\frac{k_z^2}{k_0^2}-1\right) + \frac{(k_x^2+k_y^2)^2}{k_0^2 k_e^2} = 0. \quad (11)$$

And using the relationship

$$\frac{1}{k_0^2 k_e^2} = \frac{1}{4}\left[\left(\frac{1}{k_0^2}+\frac{1}{k_e^2}\right)^2 - \left(\frac{1}{k_0^2}-\frac{1}{k_e^2}\right)^2\right], \quad (12)$$

we obtain

$$\left(\frac{k_z^2}{k_0^2}-1+\frac{k_x^2+k_y^2}{k_e^2}\right)\left(\frac{k_z^2}{k_0^2}-1+\frac{k_x^2+k_y^2}{k_0^2}\right)=0, \quad (13)$$

where the first multiplier is an ellipsoid of revolution with semiaxes k_0 and k_e, and the second one corresponds to a sphere of radius k_0. Therefore, Eq. (13) characterizes the surfaces of a uniaxial crystal.

The model used in this study determines the distribution of diffracted fields. Distribution of the light field in diffraction orders is characterized by transfer functions. These functions were derived under the assumption that the AO interaction is linear with respect to the light field. The spectral method [14,20,33], which involves expansion of the field of the light wave incident on the AO cell into a spectrum of plane waves, may be used in this case. It was also assumed that all acts of plane wave diffraction are independent. In the case of double interaction, when a plane optical wave is diffracted by a plane monochromatic acoustic wave, the diffracted beams are also plane waves, and their amplitudes are written as

$$\begin{aligned} V_0(\theta_i) &= V_{\text{inc}}(\theta_i)H_0(\theta_i);\\ V_1(\theta_i+q/k) &= V_{\text{inc}}(\theta_i)H_1(\theta_i);\\ V_2(\theta_i+2q/k) &= V_{\text{inc}}(\theta_i)\mathrm{H}_2(\theta_i), \end{aligned} \quad (14)$$

where V_0, V_1, and V_2 are the amplitudes of the fields of the zeroth, first, and second diffraction orders; V_{inc} is the amplitude of the incident light; θ_i is the orientation angle of the incident plane wave; q and k are the wave numbers of the acoustic and optical plane waves; and H_0, H_1, and H_2 are the transfer functions of the zeroth, first, and second orders.

Figure 2 shows a calculated 2D transfer function of the first diffraction order under the assumption that it coincides with the distribution $|V_1|$. The transfer function is obtained by solving the system in Eq. (6) with boundary conditions $V_0=1$ and $V_1=V_2=0$ at $z=0$. It was assumed that optical radiation at 0.63 μm diffracts on the slow acoustic wave (which propagates in a TeO_2 crystal at the velocity of 0.617×10^5 cm/s) with the frequency close to two-phonon resonance.

The angular dimensions in Fig. 2 correspond to $\sim2^\circ\times2^\circ$. The Raman–Nath parameter ν was taken equal to $\sim4\sqrt{2}\pi$, which corresponds to acoustic power in our experiment. The length $L=6$ mm. The image in Fig. 2 is an ensemble of elliptical fringes, which result from the interference of the first-order diffraction beam with the beams diffracted into the first order from the zeroth and second orders. Domains with substantial inhomogeneity are seen in the fringe image. The fringes are strongly distorted, and their distribution is actually two-dimensional. One such domain is marked by a square and used as a mask for optical Fourier processing.

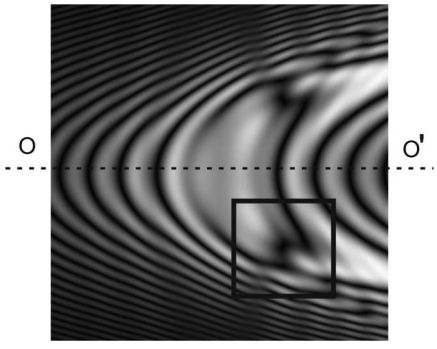

Fig. 2. Transfer function of the first diffraction order $|V_1|$ formed as the result of two-phonon Bragg diffraction. Dark regions correspond to minimum field distribution, and light regions correspond to maximum distribution.

In Fig. 3 numerical results of fast Fourier transformation (FFT) processing are presented for images of (a) rectangular, (b) circle, and (c) figure "68" by use of the transfer function $|V_1|$ (Fig. 2). One can see that in all cases sufficiently clear 2D edges are formed. Hence, in general, the mask presented by the distribution of Fig. 2 can be used as 2D spatial low-cut filter despite its sufficiently large inhomogeneity.

The theoretical results were verified experimentally. The experimental setup is presented in Fig. 4. A wide optical beam is directed on a screen with aperture P_{in}, which serves as the initial image. The radiation transmitted through the aperture is directed onto lens L_1 with the focal distance of 16 cm. The AO cell is mounted behind lens L_1 and serves as a filter of spatial frequencies. An acoustic wave propagates in the cell orthogonally to the optical beam. The cell operates in the double Bragg diffraction mode. Optical beams leaving the AO cell are directed to lens L_2 identical to L_1. The images obtained after Fourier processing are observed on screen P_{out}. To improve the

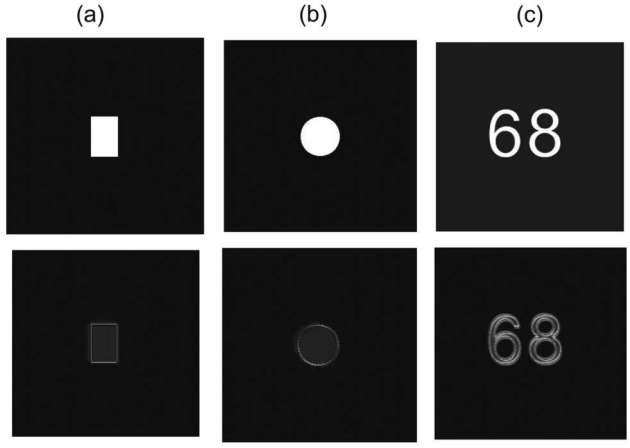

Fig. 3. Results of FFT processing for (a) rectangular, (b) circular holes and (c) figure "68" images with the transfer function shown in Fig. 2.

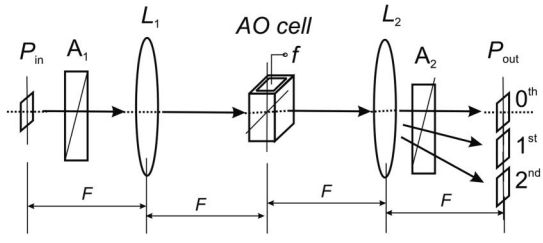

Fig. 4. Experimental setup for Fourier processing.

image quality, polarizers A_1 and A_2 are used in some experiments. Two-phonon and three-phonon diffractions were investigated without polarizers. We will show below that in the experiments with eigenmodes, superposition of the polarizers is very important.

The distances between P_{in}, L_1, the AO cell, L_2, and P_{out} are equal to focal distance. Lenses L_1 and L_2 perform the first and second Fourier transforms; in the latter case, the transform is equivalent to the inverse Fourier transform with coordinate inversion [34,35]. Three images formed in the 0th, +1st, and +2nd diffraction orders are observed on screen P_{out}. The intensity distributions of these images may be altered by changing acoustic frequency, the acoustic power, and the angular orientation of the AO cell. The initial image was either a rectangular hole of the size 1 × 1.5 mm or a circular hole 1.0 mm in diameter. The holes were illuminated from one side by wide radiation of a He–Ne laser ($\lambda = 0.63$ μm), which then directed to an input lens L_1. The AO cell is made of TeO_2 crystal. The voltage applied to a piezoelectric transducer was 5.0 V, and the frequency of an ultrasound wave was 35.5 MHz. By angular adjustment of the AO cell in the diffraction plane and in the orthogonal plane, we obtained a 2D edge of the image in the first order.

Figure 5 shows photographs of the images of zeroth and first diffraction orders on the output screen. One can see a clear 2D edge, which is formed in the first diffraction order. In other words, the experiment confirms that in accordance with the theoretical conclusion, two-phonon AO diffraction makes it possible to enhance a 2D edge of an image in the first diffraction order.

The polarization features of the 2D image edge enhancement are investigated in our paper [36]. In the experimental setup, the polarizers A_1 and A_2 are used. It is shown that the change in sound power varies the first-order diffraction's transfer function constructed in different polarization states, thus modifying the conditions of the formation of image edges depending on both the output radiation polarization and the sound wave power. For example, in some position of polarizer A_2 a contour of image is observed, while after rotation of A_2 at angle 90°, the contour disappeared. It is interesting to note that contour appears again at other voltage applied to the AO cell. A theory was developed to explain this phenomenon [36].

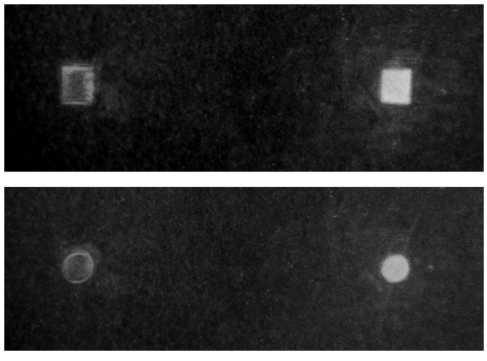

Fig. 5. Photographs of rectangular and circular holes after experimental Fourier processing. Right and left images correspond to the zeroth and first diffraction order, respectively.

The similar results were also obtained for three-phonon Bragg diffraction [37]. This diffraction in a gyrotropic crystal is described by the following set of differential equations:

$$\begin{aligned}
\frac{dV_0}{dz} &= -\frac{\nu_a}{2L} f_{01} V_1 \exp(-i\Delta k_0 z),\\
\frac{dV_1}{dz} &= \frac{\nu_a}{2L} f_{10} V_0 \exp(i\Delta k_0 z) - \frac{\nu_i}{2L} f_{12} V_2 \exp(-i\Delta k_1 z),\\
\frac{dV_2}{dz} &= \frac{\nu_i}{2L} f_{21} V_1 \exp(i\Delta k_1 z) - \frac{\nu_a}{2L} f_{23} V_3 \exp(-i\Delta k_2 z),\\
\frac{dV_3}{dz} &= \frac{\nu_a}{2L} f_{32} V_2 \exp(i\Delta k_2 z).
\end{aligned} \tag{15}$$

Here, V_0, V_1, V_2, and V_3 are the amplitudes of the zeroth, first, second, and third diffraction orders, respectively; z is the direction of evolution of the AO interaction (in our case, it coincides with the direction of optical axis Z of the crystal); ν_a and ν_i are Raman–Nath parameters for the anisotropic and isotropic diffraction, respectively (in accordance with [1], we assumed that $\nu_a = 2\nu_i$). L is the length of the AO interaction, and Δk_0, Δk_1, and Δk_2 are the magnitudes of mismatch vectors. Coefficients f_{10}, f_{01}, f_{12}, f_{21}, f_{32}, and f_{23} take into account the ellipticity of interacting waves and are defined in accordance with Eq. (7).

The system in Eq. (15) may have an analytical solution. Let us find a partial solution of Eq. (15) in a form of [38]

$$\begin{aligned}
V_0 &= \overline{a}\exp(i\alpha z); \qquad V_1 = \overline{b}\exp(i\beta z),\\
V_2 &= \overline{c}\exp(i\gamma z); \qquad V_3 = \overline{d}\exp(i\delta z),
\end{aligned} \tag{16}$$

where $\overline{a}$, $\overline{b}$, $\overline{c}$, $\overline{d}$, α, β, γ, δ are arbitrary constants. We must find these constants so that the functions in Eq. (16) would satisfy Eq. (15). Now put Eq. (16) in Eq. (15),

$$\begin{aligned}
i\alpha\overline{a}\exp(i\alpha z) &= -A_1\overline{b}\exp[i(\beta-\Delta k_0)z],\\
i\beta\overline{b}\exp(i\beta z) &= A_1\overline{a}\exp[i(\alpha+\Delta k_0)z] - A_2\overline{c}\exp[i(\gamma-\Delta k_1)z],\\
i\gamma\overline{c}\exp(i\gamma z) &= A_2\overline{b}\exp[i(\beta+\Delta k_1)z] - A_3\overline{d}\exp[i(\delta-\Delta k_2)z],\\
i\delta\overline{d}\exp(i\delta z) &= A_3\overline{c}\exp[i(\gamma+\Delta k_2)z],
\end{aligned} \tag{17}$$

where $A_1 = \frac{\nu_a}{2L} f_{01}$, $A_2 = \frac{\nu_i}{2L} f_{12}$, $A_3 = \frac{\nu_a}{2L} f_{32}$.

Each Eq. (17) should be fulfilled at any z. Now we have relationship for the exponent coefficients,

$$\begin{aligned}
&\alpha = \beta - \Delta k_0; \qquad \beta = \alpha + \Delta k_0 = \gamma - \Delta k_1;\\
&\gamma = \beta + \Delta k_1 = \delta - \Delta k_2; \qquad \delta = \gamma + \Delta k_2.
\end{aligned} \tag{18}$$

Under the conditions in Eq. (18), Eq. (17) transforms into Eq. (19),

$$\begin{aligned}
i\alpha\overline{a} + A_1\overline{b} &= 0,\\
i\beta\overline{b} - A_1\overline{a} + A_2\overline{c} &= 0,\\
i\gamma\overline{c} - A_2\overline{b} + A_3\overline{d} &= 0,\\
i\delta\overline{d} - A_3\overline{c} &= 0.
\end{aligned} \tag{19}$$

This is a system of homogeneous equations in respect to $\overline{a}$, $\overline{b}$, $\overline{c}$, and $\overline{d}$. It has nonzero solution when the determinant is equal to zero,

$$\mathrm{Det} = \begin{vmatrix} i\alpha & A_1 & 0 & 0 \\ -A_1 & i\beta & A_2 & 0 \\ 0 & -A_2 & i\gamma & A_3 \\ 0 & 0 & -A_3 & i\delta \end{vmatrix} = 0. \quad (20)$$

From Eq. (18), let us write β, γ, δ over α,

$$\beta = \alpha + \Delta k_0; \qquad \gamma = \alpha + \Delta k_0 + \Delta k_1;$$
$$\delta = \alpha + \Delta k_0 + \Delta k_1 + \Delta k_2. \quad (21)$$

Substituting Eq. (21) in Eq. (20), we obtain a fourth-order equation in respect to α,

$$\alpha^4 + B_3\alpha^3 + B_2\alpha^2 + B_1\alpha + B_0 = 0, \quad (22)$$

where $B_3 = 3\Delta k_0 + 2\Delta k_1 + \Delta k_2$,

$$B_2 = (\Delta k_0 + \Delta k_1)(\Delta k_0 + \Delta k_1 + \Delta k_2) + \Delta k_0(2\Delta k_0 + 2\Delta k_1 + \Delta k_2) - (A_1^2 + A_2^2 + A_3^2),$$
$$B_1 = \Delta k_0(\Delta k_0 + \Delta k_1)(\Delta k_0 + \Delta k_1 + \Delta k_2) - A_1^2(2\Delta k_0 + 2\Delta k_1 + \Delta k_2) - A_2^2(\Delta k_0 + \Delta k_1 + \Delta k_2) - A_3^2\Delta k_0,$$
$$B_0 = A_1^2[A_3^2 - (\Delta k_0 + \Delta k_1)(\Delta k_0 + \Delta k_1 + \Delta k_2)]. \quad (23)$$

By solving Eq. (22) we obtain four roots α_k, where «k» is "running" from 1 to 4.

The general solution for amplitudes is now written as

$$V_0 = \overline{a}_1 \exp(i\alpha_1 z) + \overline{a}_2 \exp(i\alpha_2 z) + \overline{a}_3 \exp(i\alpha_3 z) + \overline{a}_4 \exp(i\alpha_4 z),$$
$$V_1 = \overline{b}_1 \exp(i\beta_1 z) + \overline{b}_2 \exp(i\beta_2 z) + \overline{b}_3 \exp(i\beta_3 z) + \overline{b}_4 \exp(i\beta_4 z),$$
$$V_2 = \overline{c}_1 \exp(i\gamma_1 z) + \overline{c}_2 \exp(i\gamma_2 z) + \overline{c}_3 \exp(i\gamma_3 z) + \overline{c}_4 \exp(i\gamma_4 z),$$
$$V_3 = \overline{d}_1 \exp(i\delta_1 z) + \overline{d}_2 \exp(i\delta_2 z) + \overline{d}_3 \exp(i\delta_3 z) + \overline{d}_4 \exp(i\delta_4 z). \quad (24)$$

For the next calculations, we shall use the boundary conditions in a form of

$$V_0 = 1, \qquad V_1 = V_2 = V_3 = 0 \quad \text{under} \quad z = 0. \quad (25)$$

Then, Eq. (24) is now

$$1 = \overline{a}_1 + \overline{a}_2 + \overline{a}_3 + \overline{a}_4,$$
$$0 = \overline{b}_1 + \overline{b}_2 + \overline{b}_3 + \overline{b}_4,$$
$$0 = \overline{c}_1 + \overline{c}_2 + \overline{c}_3 + \overline{c}_4,$$
$$0 = \overline{d}_1 + \overline{d}_2 + \overline{d}_3 + \overline{d}_4. \quad (26)$$

By using Eq. (19) and Eq. (21) we may write $\overline{b}_k$, $\overline{c}_k$, $\overline{d}_k$ over α_k and $\overline{a}_k$,

$$\overline{b}_k = -\frac{i\alpha_k\overline{a}_k}{A_1}; \qquad \overline{c}_k = \frac{\overline{a}_k}{A_2}\left[A_1 - \frac{\alpha_k(\alpha_k + \Delta k_0)}{A_1}\right],$$
$$\overline{d}_k = -i\overline{a}_k\frac{A_3}{A_2(\alpha_k + \Delta k_0 + \Delta k_1 + \Delta k_2)}\left[A_1 - \frac{\alpha_k(\alpha_k + \Delta k_0)}{A_1}\right]. \quad (27)$$

After substitution of Eq. (27) into Eq. (26), we get a system of linear equations with unknown $\overline{a}_k$. By solving this system, we shall find all parameters to calculate amplitudes of V_0, V_1, V_2, and V_3 from Eq. (24) under condition $z = L$. These amplitudes should satisfy the conservation low for any z,

$$V_0V_0^* + V_1V_1^* + V_2V_2^* + V_3V_3^* = 1. \quad (28)$$

Figure 6 shows the domain of 2D transfer function of the first order, which allows obtaining the 2D contour of an image.

The acoustic frequency at which triple diffraction occurs was chosen to be 26.33 MHz. The mathematical model of the surfaces of wave vectors was based on Eqs. (8)–(10). Theoretical investigations show that the obtained transfer function allows us to extract the 2D contour of an optical image. Let us say that images represented in Fig. 3 transform into their contours after applying the transfer function Fig. 6.

These theoretical results were verified experimentally [37]. The contour of the rectangular using the AO cell of TeO_2 in which the acoustic wave propagates with the frequency 26.3 MHz and applied voltage of 2.7 V was also obtained.

The possibility of formation of the edge of a 2D optical image in two diffraction orders (first and second) simultaneously by means of Fourier processing with the use of triple Bragg diffraction is demonstrated theoretically and experimentally [39].

Taking these arguments into account, now we can make the conclusion that the multi-phonon Bragg diffraction is the effective method for processing of the 2D images. From a physical point of view, the proposed method is based on the superposition of two AO fields with similar polarizations but different amplitude and phase distributions. This phenomenon has been taken into account in the sets of Eqs. (6) and (15). As a result, the fields of the "intermediate" orders are normally very inhomogeneous, while some domains possess the 2D properties. Such domains can be in several places of the field. For example, in Fig. 6, besides the marked domain there is analogous

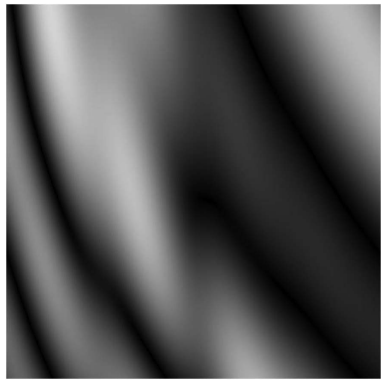

Fig. 6. Transfer function of first diffraction order forming as a result of triple diffraction.

domain that is symmetrically located in respect to the O–O′ axis. It should be added that configuration and position of the "proper" domains depend on the acoustic power [40]. Forming of the inhomogeneous domains can occur not only in intermediate orders but in the zeroth and highest order as well. It is caused by the influence of the fields of "neighbor's" orders with inhomogeneous distributions. For example, we investigate the image edge enhancement with second diffraction order in the two-phonon diffraction process in [41]. Thus, transfer function was obtained; the experiments confirmed the possibility of 2D image contours forming by the highest diffraction order.

3. TRANSFER FUNCTIONS AS SUPERPOSITION OF THE FIELDS WITH ORTHOGONAL POLARIZATIONS

In this section, we consider the transfer function forming as a superposition of the eigen optical modes of the crystal. Note that the polarization of the eigenmodes is orthogonal with respect to each other. The vector diagram of two versions of AO diffraction, which involve the simultaneous diffraction of both optical modes on the single acoustic wave, is presented in Fig. 7. An incident beam with wave vector **K** falls on the input optical face OX of the crystal. Inside the crystal, the beam splits into two eigenmodes with wave vectors $\mathbf{K}_1$ and $\mathbf{K}_2$. These beams diffract on the acoustic wave with wave vector **q**. Both beams diffract on the one side in respect to the incident beam, Fig. 7(a); otherwise, they diffract on both sides, Fig. 7(b). In the first case $\mathbf{K}_1$ or $\mathbf{K}_2$ diffracts into $\mathbf{K}_3$ and $\mathbf{K}_4$; in the second case beam $\mathbf{K}_1$ diffracts into $\mathbf{K}_3$, and $\mathbf{K}_2$ into $\mathbf{K}_4$. The diffraction presented in Fig. 7(a) is described by the set of equations [42]

$$\begin{aligned}
\frac{dV_1}{dz} &= -\frac{\nu_i}{2L} f_{14} V_4 \exp(i\Delta k_3 z) - \frac{\nu_a}{2L} f_{13} V_3 \exp(i\Delta k_2 z),\\
\frac{dV_2}{dz} &= -\frac{\nu_i}{2L} f_{23} V_3 \exp(i\Delta k_1 z)\\
&\quad -\frac{\nu_a}{2L} f_{24} V_4 \exp[i(\Delta k_1 + \Delta k_2 + \Delta k_3) z],\\
\frac{dV_3}{dz} &= \frac{\nu_i}{2L} f_{32} V_2 \exp(-i\Delta k_1 z) + \frac{\nu_a}{2L} f_{31} V_1 \exp(-i\Delta k_2 z),\\
\frac{dV_4}{dz} &= \frac{\nu_i}{2L} f_{41} V_1 \exp(-i\Delta k_3 z)\\
&\quad + \frac{\nu_a}{2L} f_{42} V_2 \exp[-i(\Delta k_1 + \Delta k_2 + \Delta k_3) z]. \qquad (29)
\end{aligned}$$

It should be noted that with this approach, the system of Eq. (29) also has analytical solution.

It is assumed that the amplitudes of beams $\mathbf{K}_1$ and $\mathbf{K}_2$ before entering into the region of AO interaction are equal, therefore by solving the system of Eq. (29) we use the boundary conditions $V_1 = V_2 = (\sqrt{2})^{-1}$, $V_3 = V_4 = 0$ at $z = 0$.

It is known that the combining of two circularly polarized waves with equal amplitudes rotating in opposite directions leads to linearly polarized wave [43]. If the velocities of waves are different, then the angle of rotation of linear polarization varies as a function the crystal length. In addition, when the wave amplitudes are not equal to each other, the total wave will be elliptically polarized rather than linear. Our calculations take into account the extracting of the linear polarization component at the output of the optical system. The optimal position of polarizer A_2 determines the best quality of image contour. The orientation of polarizer is measured by the angle α, which is counted in respect to the propagation direction of acoustic wave. The theoretical analysis shows that the polarizer significantly improves the AO filter characteristics.

Example of transfer function of the zeroth Bragg order calculated by solving the system in Eq. (16) with allowance for Eqs. (2)–(6) for $\alpha = 100°$ and $P_a = 1.5$ W is shown in Fig. 8. Diffraction occurs in TeO_2 crystal at the frequency of acoustic wave of 26 MHz. The angular size of the field in Fig. 8 is 15° × 15°. The field represents a family of circles with a single center and several inhomogeneous domains caused by AO interaction. Two domains are marked by squares which, according to our analysis, are suitable for obtaining a 2D image edge. The domains are located symmetrically in respect to the axis $O - O'$. It should be noted that transfer function of the zeroth order is formed by two different physical mechanisms, i.e., the conoscopic effect and the acousto-optic interaction.

It can also be seen that both isotropic and anisotropic diffraction are involved in Eqs. (16). By fitting the voltage of a high-frequency signal applied to transducer (in our case, optimum voltage was 7.8 V), angular orientation of AO cell, sound frequency of 26.6 MHz, and angle of polarizer inclination of $\alpha \approx 45°$, the 2D image edge enhancement in the zeroth diffraction order was clearly observed [42].

Let us consider case (b) in Fig. 7. Here the eigenmodes $\mathbf{K}_1$ and $\mathbf{K}_2$ diffract on different sides in respect to incident beam **K**. This version is similar to the polarization-independent AO light

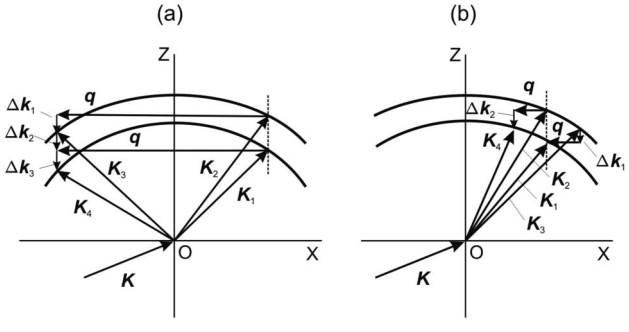

Fig. 7. Vector diagram of two versions of the AO diffraction.

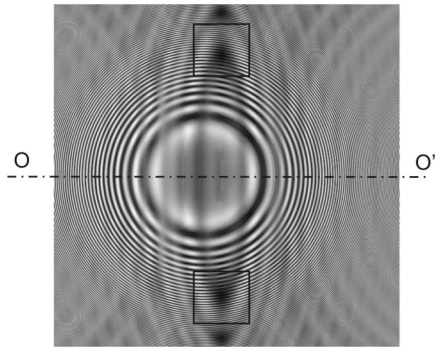

Fig. 8. Transfer function of the zeroth diffraction order. Beams diffract on the one side in respect to the incident light.

modulation [44], which gives rise to elaboration of different AO devices (see for example [45–50]). But in these papers, it was used in the case when the beams $\mathbf{K}_1$ and $\mathbf{K}_2$ propagate collinearly to each other. In our case, the beams are not collinear; they refract at different angles on the face OX. At the same time, the projections of $\mathbf{K}_1$ and $\mathbf{K}_2$ on the face OX are equal toeach other in accordance with the refraction law [43]. Beam $\mathbf{K}_1$ diffracts into $\mathbf{K}_3$ with the vector mismatch Δk_1, and $\mathbf{K}_2$ diffracts into $\mathbf{K}_4$ with the vector mismatch Δk_2. The acts of diffraction occur independently and are described by well-known equations [1–3]. At the output of the crystal, beams $\mathbf{K}_1$ and $\mathbf{K}_2$ are collinear and form the zeroth diffraction order. Beams $\mathbf{K}_3$ and $\mathbf{K}_4$ are −1st and +1st orders of diffraction, respectively. Figure 9 represents the distribution of the zeroth diffraction order as a result of superposition of fields $\mathbf{K}_1$ and $\mathbf{K}_2$ with taking into account the shift of beams inside of the crystal. The angle of the polarizer A_2 was taken equal to 45°. As before, diffraction occurs on a "slow" acoustic wave, but the frequency was 9 MHz. The angular size of field is 10° × 10°. As in the previous case, the field represents a family of circles. The domain is marked out by square, which, according to our analysis, is suitable to obtain the 2D contour of the image. The mask of Fig. 9 results in FFT processing of images, which are similar to the cases shown in Fig. 3. The results of the experiment are shown in Fig. 10 where the photographs of the rectangular hole after experimental optical Fourier processing are presented. The picture above is the image observing on the output screen without an acoustic wave, and the picture below is when the acoustic power turns on. In the middle of low picture, the zeroth diffraction order is shown; on the right and left sides +1 and −1 orders are shown. The voltage applied to the transducer was 3.9 V and frequency of acoustic wave 9 MHz. It can be seen that image contour of the zeroth order has very good quality. Hence, the proposed case of diffraction can be successfully used for image edge enhancement processing.

It should be noted that similar investigations were made with the use of two transfer functions for the Fourier processing [16,51–54]. However, in these investigations, light crosses two different acoustic fields. In our case, the light crosses only one field. The final result depends only on AO process peculiarities and on the properties of AO media and not on the number of acoustic fields. The use of a single AO cell instead of several offers a lot of advantages: the absence of inter-modulation processes, a minimum of light loses due to scattering or reflection of light from crystal faces, minimal cell dimensions and supplied electrical power, etc.

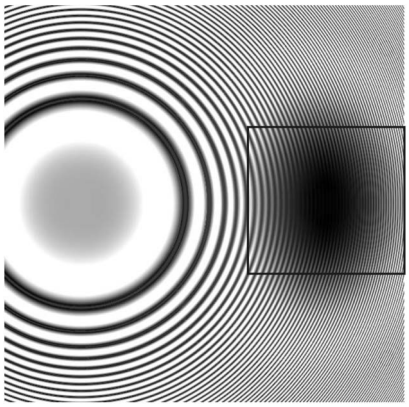

Fig. 9. Transfer function of the zeroth diffraction order. Beams diffract on the different sides in respect to the incident light.

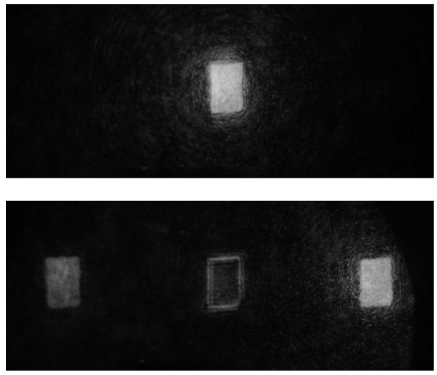

Fig. 10. Photographs of rectangular hole after experimental Fourier processing. Above: image without acoustic power; below: acoustic power turns on.

4. CONCLUSION

AO image processing is determined by the transfer function of AO interaction. In this paper, we have examined a new approach for formation of the transfer function based on the superposition of two AO fields with similar and orthogonal polarizations. For example, the case when the fields have similar polarization takes place for multi-phonon Bragg diffraction. In common cases, the superposition of the fields with different amplitude and phase distributions leads to a very inhomogeneous field; some domains of the field possess 2D properties. The position and configuration of domains can be changed by a variation of acoustic frequency and power. In this paper, we have described the transfer functions forming in the "intermediate" diffraction orders. But this process is possible in the zeroth and highest order as well. It is caused by influence of the fields of "neighbor's" orders with inhomogeneous distributions.

A case when transfer function is formed as a superposition of two AO fields with orthogonal polarizations takes place, for example, in the process simultaneous diffraction of two eigenmodes of crystal on a single acoustic wave. Two versions of such diffraction when diffracted beams propagate on one side and on both sides in respect to the incident beam are proposed and investigated.

It should be noted that not every domain with the inhomogeneous field distribution is proper for the 2D processing and therefore has to be checked by FFT processing. In our study, we carried out this procedure for each domain and selected only the domains with the desired properties. All obtained theoretical results were confirmed experimentally.

Generally speaking, the AO transfer functions can be formed by other methods; for instance, considering two-dimensional AO diffraction or AO diffraction on several acoustic waves. But the advantage of our approach is the use of

one-dimensional AO diffraction equations on the base of single acoustic wave for the calculation of two-dimensional AO transfer functions.

Though the theory of proposed cases is more complicated in comparison with the "common" Bragg diffraction into one order, the experimental realization of these versions is no more intricate at all.

Funding. Russian Foundation for Basic Research (RFBR) (15-07-02312)

Acknowledgment. This paper is based on the talk presented at the 13th School on Acousto-Optics and Applications, Moscow, Russia, 19–23 June 2017. Vladimir M. Kotov, Gennady N. Shkerdin, and Stanislav V. Averin, "Acousto-optic filters using multi-phonon Bragg diffraction," Program and Abstracts Book, p. 41.

REFERENCES

1. V. I. Balakshy, V. N. Parygin, and L. E. Chirkov, *Physical Principles of Acousto-Optics* (Radio & Svyaz, 1985).
2. A. Korpel, *Acousto-Optics*, 2nd ed. (Marcel Dekker, 1996).
3. J. Xu and R. Stroud, *Acousto-Optic Devices* (Wiley, 1992).
4. L. N. Magdich and V. Y. Molchanov, *Acoustooptical Devices and Their Application* (Gordon and Breach Science, 1989).
5. L. N. Magdich and V. Y. Molchanov, "Diffraction of a divergent beam by intense acoustic waves," Opt. Spectrosc. **42**, 533–539 (1977).
6. R.-S. Chu, J. A. Kong, and T. Tamir, "Diffraction of Gaussian beams by periodically modulated layer," J. Opt. Soc. Am. **67**, 1555–1561 (1977).
7. R. Whitman, A. Korpel, and S. Lotsoff, "Application of acoustic Bragg diffraction to optical processing techniques," in *Proceedings of the Symposium on Modern Optics* (Wiley, 1967), pp. 243–246.
8. V. I. Balakshy, "Scanning of images," Sov. J. Quantum Electron. **6**, 965–971 (1979).
9. V. I. Balakshy, "Acousto-optic cell as a filter of spatial frequencies," Radiotekh. Elektron. **29**, 1610–1616 (1984).
10. M. R. Chatterjee, T.-C. Poon, and D. N. Sitter, Jr., "Transfer function formalism for strong acousto-optic Bragg diffraction of light beams with arbitrary profiles," Acoustica **71**, 81–92 (1990).
11. P. P. Banerjee and C.-W. Tarn, "A Fourier transform approach to the acoustooptic interactions in the presence of propagational diffraction," Acoustica **74**, 181–191 (1991).
12. J. Xia, D. B. Dunn, T.-C. Poon, and P. P. Banerjee, "Image edge enhancement by Bragg diffraction," Opt. Commun. **128**, 1–7 (1996).
13. D. Casasent, *Optical Data Processing Applications* (Springer, 1978).
14. J. W. Goodman, *Introduction to Fourier Optics* (McGraw-Hill, 1968).
15. P. P. Banerjee, D. Cao, and T.-C. Poon, "Basic image processing operations by use of acousto-optics," Appl. Opt. **36**, 3086–3089 (1997).
16. D. Cao, P. P. Banerjee, and T.-C. Poon, "Image edge enhancement using two cascaded acousto-optic cells with contra-propagating sound," Appl. Opt. **37**, 3007–3014 (1998).
17. P. P. Banerjee, D. Cao, and T.-C. Poon, "Notch spatial filtering with an acousto-optic modulator," Appl. Opt. **37**, 7532–7537 (1998).
18. V. I. Balakshy, K. R. Asratyan, and V. Y. Molchanov, "Acoustooptic collinear diffraction of a strongly divergent optical beam," Pure Appl. Opt. **3**, S87–S92 (2001).
19. V. I. Balakshy and D. E. Kostyuk, "Application of acousto-optic selectivity for optical image processing," Proc. SPIE **5828**, 95–104 (2004).
20. V. I. Balakshy and V. B. Voloshinov, "Acousto-optic image processing in coherent light," Quantum Electron. **35**, 85–90 (2005).
21. V. I. Balakshy, V. B. Voloshinov, T. M. Babkina, and D. E. Kostyuk, "Optical image processing by means of acousto-optic spatial filtration," J. Mod. Opt. **52**, 1–20 (2005).
22. V. I. Balakshy and D. E. Kostyuk, "Spatial structure of acousto-optic phase matching in uniaxial crystals," Opt. Spectrosc. **101**, 283–289 (2006).
23. V. I. Balakshy and D. E. Kostyuk, "Acousto-optic image processing," Appl. Opt. **48**, C24–C32 (2009).
24. I. C. Chang, "Noncollinear acousto-optic filter with large angular aperture," Appl. Phys. Lett. **25**, 370–372 (1974).
25. V. N. Belyi and V. V. Shepelevich, "Diffraction of light on ultrasound in gyrotropic absorbing crystals," Opt. Spektrosc. **52**, 842–846 (1982).
26. V. Y. Rakovskii and A. S. Shcherbakov, "Multi phonon Bragg scattering of light on the acoustic waves," Zh. Tekh. Fiz. **60**, 107–114 (1990).
27. L. D. Landau and E. M. Lifshitz, *Electrodynamics of Continuous Media* (Pergamon, 1984).
28. A. Yariv and P. Yeh, *Optical Waves in Crystals* (Wiley, 1984).
29. Y. I. Sirotin and M. P. Shaskol'skaya, *Osnovy kristallofiziki (Principles of Crystal Physics)* (Nauka, 1975).
30. V. M. Kotov, G. N. Shkerdin, and A. N. Buliuk, "Two-dimensional image edge enhancement by two-phonon Bragg diffraction," Sov. J. Quantum Electron. **41**, 1109–1113 (2011).
31. V. M. Kotov, "High frequency two-color splitting of laser radiation," Opt. Spektrosc. **77**, 493–497 (1994).
32. V. M. Kotov, *Acousto-Optics. Bragg Diffraction of the Multi-Color Radiation* (Yanus-K, 2016).
33. A. K. Ghatak and K. Thyagarajan, *Contemporary Optics* (Plenum, 1978).
34. T. S. Francis and I.-C. Khoo, *Principles of Optical Engineering* (Wiley, 1990).
35. A. A. Akaev and S. A. Maiorov, *Optical Methods of Information Processing* (Vysshaya Shkola, 1988).
36. V. M. Kotov, G. N. Shkerdin, and V. I. Grigor'evskii, "Polarization features of the 2D contouring of an optical image under double Bragg diffraction conditions," Sov. Zh. Radio Techn. Electr. **58**, 226–232 (2013).
37. V. M. Kotov and G. N. Shkerdin, "Formation of the two-dimensional contour of an image during triple Bragg diffraction," Sov. Zh. Radio Techn. Electr. **58**, 1011–1014 (2013).
38. C. Chicone, *Ordinary Differential Equations with Applications* (Springer, 1999).
39. V. M. Kotov, G. N. Shkerdin, and S. V. Averin, "Formation of the two-dimensional image edge in two diffraction orders in the process of triple Bragg diffraction," Sov. Zh. Radio Techn. Electr. **61**, 1275–1279 (2016).
40. V. M. Kotov, G. N. Shkerdin, S. V. Averin, and E. V. Kotov, "Effect of the acoustic power on the forming process of the optical image edge enhancement," Prikl. Fiz. **3**, 5–8 (2012).
41. V. M. Kotov, G. N. Shkerdin, and S. V. Averin, "Two-dimensional image edge enhancement with the using of the diffraction into second Bragg order," Radiotechnika. **12**, 57–61 (2012).
42. V. M. Kotov, S. V. Averin, P. I. Kuznetsov, and E. V. Kotov, "Acousto-optic method of spatial frequency filtration based on diffraction of two eigenmodes of a crystal," Sov. J. Quantum Electron. **47**, 665–668 (2017).
43. M. Born and E. Wolf, *Principles of Optics* (Pergamon, 1964).
44. H. Lee, "Polarization-independent acoustooptic light modulation with large angular aperture," Appl. Opt. **27**, 815–817 (1988).
45. V. B. Voloshinov and V. Y. Molchanov, "Acousto-optical modulation of radiation with arbitrary polarization direction," Opt. Laser Technol. **27**, 307–313 (1995).
46. V. B. Voloshinov, V. Y. Molchanov, and J. C. Mosquera, "Spectral and polarization analysis of optical images by means of acoustooptics," Opt. Laser Technol. **28**, 119–127 (1996).
47. S. N. Antonov, "Acoustooptic nonpolar light controlling devices and polarization modulators based on paratellurite crystals," Tech. Phys. **49**, 1329–1334 (2004).
48. S. N. Antonov, A. V. Vainer, V. V. Proklov, and Y. G. Rezvov, "Inverse acoustooptic problem: coherent summing of optical beams into a single optical channel," Tech. Phys. **52**, 610–615 (2007).

49. V. S. Anchutkin, A. B. Bel'skii, V. B. Voloshinov, and K. B. Yushkov, "Acoustooptical method of spectral-polarization image analysis," J. Opt. Technol. **76**, 473–477 (2009).
50. V. Y. Molchanov, Y. I. Kitaev, A. I. Kolesnikov, V. N. Narver, A. Z. Rozenshtein, N. L. Solodovnikov, and K. G. Shapovalenko, *Theory and Practice of the Modern Acoustooptics* (MISiS, 2015).
51. N. Gupta and V. B. Voloshinov, "Development and characterization of two-transducer imaging acousto-optic tunable filters with extended tuning range," Appl. Opt. **46**, 1081–1088 (2007).
52. L. N. Magdich, K. B. Yushkov, and V. B. Voloshinov, "Wide-aperture diffraction of unpolarised radiation in a system of two acousto-optic filters," Sov. J. Quantum Electron. **39**, 347–352 (2009),
53. J.-C. Kastelik, K. B. Yushkov, S. Dupont, and V. B. Voloshinov, "Cascaded acoustooptical system for the modulation of unpolarized light," Opt. Express **17**, 12767–12776 (2009).
54. K. B. Yushkov, S. Dupont, J.-C. Kastelik, and V. B. Voloshinov, "Polarization-independent imaging with an acousto-optic tandem system," Opt. Lett. **35**, 1416–1418 (2010).

62.148.254.114 {ts '2018-02-22 02:59:05'}